Cold Regions Science and Technology 201 (2022) 103618

Contents lists available at ScienceDirect

Cold Regions Science and Technology

journal homepage: www.elsevier.com/locate/coldregions

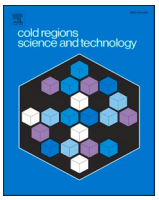

Seasonal forecasting of landfast ice in Foggy Island Bay, Alaska in support of ice road operations

Peter A. Bieniek [a,*], Hajo Eicken [a], Meibing Jin [a], Andrew R. Mahoney [b], Josh Jones [b], Uma S. Bhatt [b,c]

[a] International Arctic Research Center, University of Alaska Fairbanks, 2160 Koyukuk Dr., Fairbanks, AK 99775, USA
[b] Geophysical Institute, University of Alaska Fairbanks, 2156 Koyukuk Dr., Fairbanks, AK 99775, USA
[c] Department of Atmospheric Sciences, University of Alaska Fairbanks, 2160 Koyukuk Dr., Fairbanks, AK 99775, USA

ARTICLE INFO

Keywords:
Seasonal prediction
Landfast ice
Alaska

ABSTRACT

Landfast ice along the Arctic coasts plays an important role in supporting ecosystem services, local communities and offshore activities by industry. Seasonal predictions of landfast ice conditions are generally lacking in current seasonal forecasting products but are needed especially for planning of on-ice activities such as the construction of ice roads. This study focuses on the planned offshore development of Liberty Island where there is a need to generate seasonal forecasts for the construction of ice roads in Foggy Island Bay along the Beaufort Sea coast in northern Alaska. Due to the lack of prior in-situ observations of ice thickness in the region, a combination of newly obtained field measurements, remote sensing data analysis and modeling were employed to produce prototype seasonal forecasts of ice thickness in the landfast ice around Liberty Island. Seasonal forecasts initialized in September and March were built using Climate Forecast System seasonal forecast model data coupled with a single column ice model to forecast ice thickness that capture the start and end of the operational season, respectively. The results showed that the model forecasts had modest skill in capturing the timing of key ice thickness thresholds needed to support vehicle traffic during the start of the season in November–December but very limited skill with end of season and ice breakup forecasts. Much of the forecast skill was improved through bias correction but such improvement was hampered by the lack of long-term observational data in the region. Integration of the observational data and modeling is necessary to begin development of seasonal forecasts in this data sparse region.

1. Introduction

1.1. Motivation

Arctic landfast sea ice lines the vast majority of Arctic coastlines for a significant part of the year and constitutes an important, seasonal element of the coastal zone that supports a range of ecosystem services (Dammann et al., 2019; Eicken et al., 2009; Yu et al., 2014). In many parts of the Arctic and sub-Arctic, the landfast ice cover serves as an important platform for a range of human activities, including over-ice travel and transportation between communities (Mäkynen et al., 2020) or the harvesting of marine living resources (Ford et al., 2019). Ice roads across landfast ice also provide services to the natural resource industry, including access to offshore production sites or the staging and operation of heavy equipment associated with the construction of temporary or permanent structures (Potter and Walden, 1981; Dumas et al., 2005; Bashaw et al., 2013). Many ice charting services routinely map the extent of landfast ice using an amalgamate of different remote sensing techniques (Yu et al., 2014). Furthermore, recent advances in synthetic aperture radar (SAR) remote sensing, in particular SAR interferometry, have greatly aided large-scale mapping of landfast ice extent and stability at resolutions of hundreds of meters or less (Dammann et al., 2019; Mäkynen et al., 2020).

There is a considerable interest in seasonal forecasting of sea ice and most efforts have focused on capturing broader conditions such as sea ice extent across the pan-Arctic (e.g. Sigmond et al., 2013; Blanchard-Wrigglesworth et al., 2017). There is also growing interest in and efforts at forecasting sea ice at regional scales (Bushuk et al., 2019). However, the prediction of landfast ice formation, persistence and decay, in particular on sub-seasonal to seasonal timescales has received less

* Corresponding author.
E-mail address: pbieniek@alaska.edu (P.A. Bieniek).

https://doi.org/10.1016/j.coldregions.2022.103618
Received 9 December 2021; Received in revised form 23 May 2022; Accepted 8 June 2022
Available online 14 June 2022

attention. In principle, forecasting ice growth in the coastal ice-ocean system or seasonal scale prediction of atmospheric forcing from ensemble simulations does not present fundamental challenges, although the resolving of key processes critical to landfast ice stability still requires work (e.g., Lemieux et al., 2016).

Partly, lack of research progress in this field may be tied to the lack of pressing, clearly defined information needs. For example, previous work on forecasting the decay and breakup of landfast ice at Utqiagvik in northern Alaska by Petrich et al. (2012) was motivated by a broader understanding of key processes, but did not address a specific application. This past study identified absorption of solar shortwave energy by the coastal ice-ocean system – derived from the Weather Research and Forecasting (WRF) model – as a key predictor of in-situ break-up with lead times of up to 14 days.

Here, we present a case study for seasonal-scale prediction of landfast ice formation, growth and decay at Foggy Island Bay, a semi-sheltered coastal site in the Alaska Beaufort Sea (Fig. 1). The need for long-range forecasts with lead times of weeks to months at this particular location was driven by the planned use of landfast ice to support transport of gravel for the construction of an artificial island (Liberty Island). Advance estimation of the start date and duration of an operations window, defined by the ability of the ice cover to safely support over-ice transport of a range of different heavy trucks and equipment, was explored as a measure to enhance planning of the effort and reduce costs. In our study, we drew on ice charts and SAR remote sensing data for a study of the seasonal landfast ice cycle and associated key dates at the study location. A single column ice-ocean model, forced with meteorological inputs from global climate models that produce seasonal forecasts, was used to predict ice formation, growth and decay. An ice-mass balance buoy deployed at the study site provided in-situ data for model validation. The specific predictand variables, the criteria defining safe operations windows, and the tolerable uncertainty in the predictions were identified based on the particular application, including types of transportation modes and heavy equipment used.

1.2. Background

The application that drove development of a seasonal landfast ice prediction approach was the proposed use of an ice road in the construction of a gravel island. The operating season for such ice roads depends on the timing of freeze-up, evolution of the sea ice cover – specifically its thickness, and eventual breakup of the landfast ice in Foggy Island Bay. Forecast guidance weeks to months in advance, along with a more thorough understanding of the observational record of ice conditions in the region, were needed to inform planning and operational decision-making for upcoming seasons. In particular, long-range forecasts were needed to help plan and continuously update the delivery schedule of gravel and other materials to the artificial island construction site over the course of the winter construction season. With a lack of in-situ sea-ice measurements at this particular site, the project required a coordinated effort of field measurements, remote sensing data, modeled meteorological data and a single column ice model to address the feasibility of making seasonal forecasts (Fig. 2).

Based on guidance provided by the operator, we established the need for a seasonal scale prediction of the date at which on-ice operations are safe to commence in the early ice season, and the date on which operations have to cease in the late ice season (Fig. 3). Such predictions, with lead times of >3 months prior to the season and continual updates weeks to months out, would inform planning of the construction season (E.g., can all gravel be moved within a single season?). The timing and length of the on-ice operations season would also determine timing and duration of leasing, staging and deployment of equipment and personnel.

The predictand variables for such an application were identified as (i) the dates for which given landfast ice thickness thresholds as a result of ice growth are exceeded (persisting), (ii) the dates for which ice thickness drops below those same thresholds as a result of ice melt (ablation). The thickness criteria need to be satisfied along the entire length of the ice road from shore to the construction site. Here, we assume that along an ice road perpendicular to shore, the landfast ice is

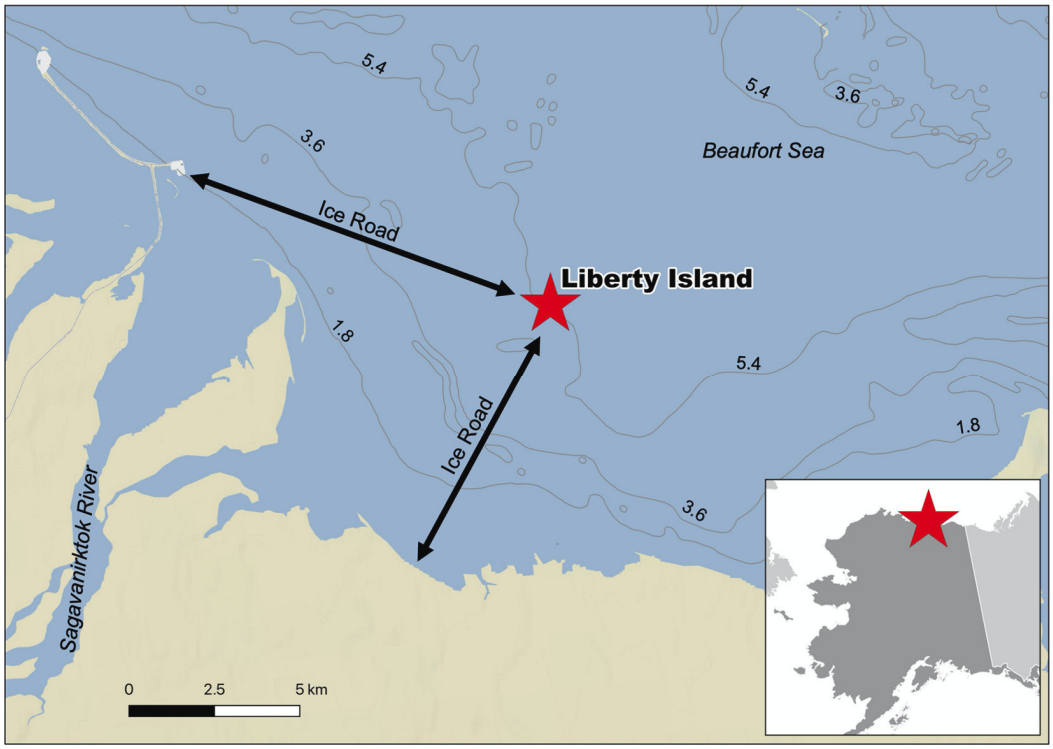

Fig. 1. Location of proposed Liberty Island development (red star) in Foggy Island Bay and approximate locations of planned ice roads (arrows). Depth isobaths derived from NOAA Electronic Navigational Charts (gray contour lines) are in meters. The location of the study area is shown by the star in the inset map. (For interpretation of the references to colour in this figure legend, the reader is referred to the web version of this article.)

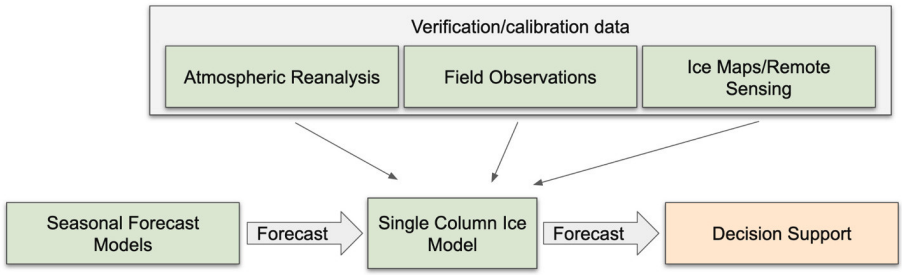

Fig. 2. Overview of project component integration.

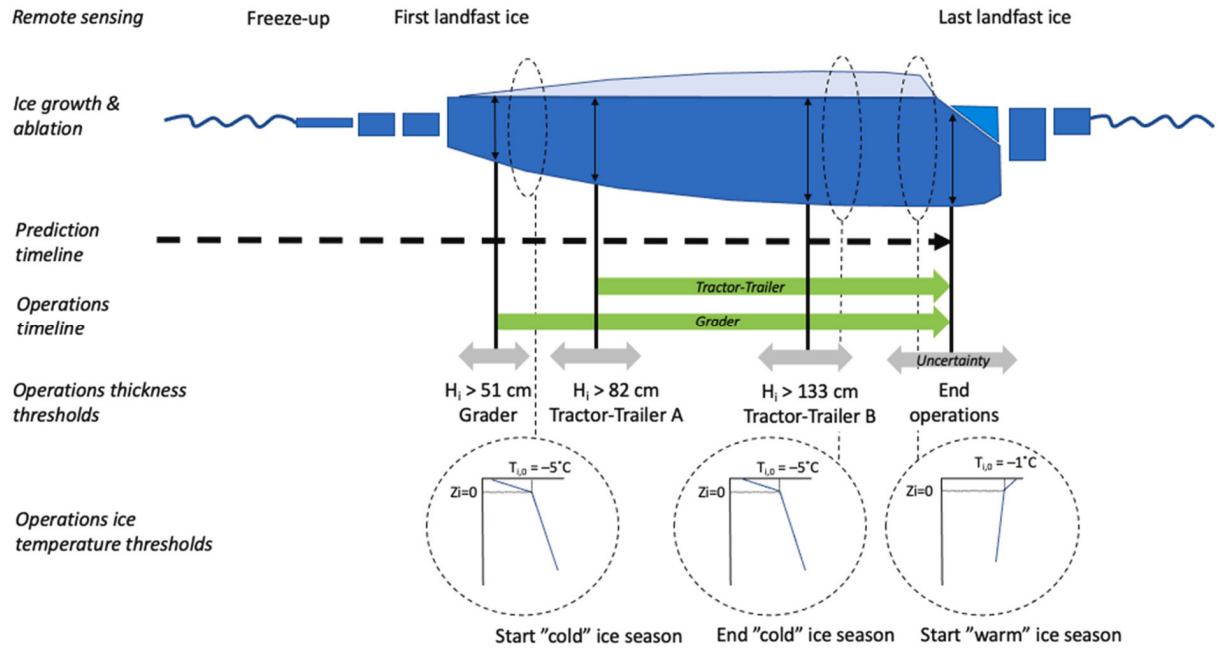

Fig. 3. Schematic of landfast ice seasonal cycle and key operational thresholds based on ice thickness and ice temperature. Also shown are specific dates derived from remote sensing data. Note that for the purposes of this study, end of operations criteria were not defined beyond a notional "last landfast ice" date tied to ice thickness dropping below 90 cm as a result of surface and bottom ablation.

thickest nearshore where it forms earliest in the season, and is thinnest at the construction site away from shore as a result of the general pattern of seaward advance and thickening of landfast ice at that location (Fig. 3). Also, both in the context of the development of a prediction model and potentially from an operations perspective, the dates that define the period of stable landfast ice absent of any ice breakout events were determined through analysis of remote-sensing imagery and ice charts (Fig. 3). For the purposes of this study, these two dates are referred to as first landfast ice and last landfast ice (Fig. 3).

Nominal ice thickness thresholds that would need to be predicted were identified based on guidance from industry manuals and established best practice for the region (BP and Golder Associates, 2013; E. Bashaw, personal communication, 2017) as summarized in Fig. 3: (i) the minimum ice thickness to allow operations of a grader (20 in./51 cm) to begin preparations for an ice road; (ii) the minimum ice thickness to support use of a medium sized tractor-trailer for gravel hauling operations (32 in./82 cm); (iii) the minimum ice thickness to support use of a heavy duty tractor-trailer (52 in./133 cm). As indicated schematically in Fig. 3 and discussed further below, the end of the ice-operations season is more difficult to define. Ice thickness as a criterion for operations may not be sufficient on its own given major changes in ice mechanical properties with ice warming and onset of melt. Hence, we identified the onset and end of the "cold" ice temperature regime as a relevant potential predictand variable provided by the model employed in this study. Drawing on BP and Golder Associates (2013), the threshold for onset/end of the cold season was defined by an ice surface temperature of −5 °C (Fig. 3).

The aim of the prediction system is to provide forecasts - in this study produced using a single column sea ice model driven by output from the National Oceanic and Atmospheric Administration (NOAA)'s Climate Forecast System model - for the critical dates identified in the operations timeline detailed in Fig. 3. The prediction uncertainty associated with the timing of each of these events (i.e., the length of the time interval that contains the observed event across a number of years relative to the spread of dates provided by the prediction system for those same years) is schematically illustrated in Fig. 3. The width of this uncertainty interval is both a function of the prediction lead time (how far in advance of the event is a prediction issued?) as well as different types of errors inherent to the prediction approach (e.g., how well are key processes driving landfast ice formation and growth captured by the single column sea ice model?). In principle, for the present application one would assume with a forecast issued on, e.g., June 1 of a given year, the uncertainty in predicting dates defining the end of on-ice operations would be larger than the uncertainty in predicting dates defining the onset of on-ice operations. However, since the processes determining ice break-up are different from those constraining ice formation and growth, this may not necessarily be the case and is explored further below.

2. Data and methods

2.1. Seasonal Ice Mass-balance Buoys (SIMBs)

In 2018 and 2019 a seasonal ice mass-balance buoy (SIMB) was deployed near the proposed Liberty Island site in Foggy Island Bay (see location in Fig. 1) for the purpose of measuring changes in the thickness (i.e. mass) of sea ice during the growth and melt seasons. The SIMB was a self-contained buoy manufactured by Cryosphere Innovations, LLC that was designed to be deployed into a hole drilled into the ice and allowed to freeze-in. It measured snow depth using a down-looking acoustic altimeter to determine the vertical position of the snow surface. Once the snow has completely melted, the same sensor is able to measure the melt of the exposed ice surface. An upward-looking acoustic altimeter below the ice measures the vertical position of the ice bottom. Together, data from the two acoustic altimeters allows for the calculation of the thickness of the sea ice. Temperature sensors spaced every 2 cm along the hull of the SIMB provided a measurement of the temperature profile through the ice and snow from the ocean to the atmosphere. The SIMB was also equipped with additional sensors to measure air and water temperature for the purpose of sound-speed corrections. Table 1 lists the deployment dates and locations for each SIMB as well as initial snow and ice measurements and notes about recovery.

2.2. Ice charts and remote sensing

In a previous study, Mahoney et al. (2014) developed a comprehensive dataset (hereafter, referred to as the M2014 dataset) of the seasonal variability in landfast ice extent from 1996 to 2008, using publicly available Radarsat synthetic aperture radar (SAR) images of the coastal waters of northern Alaska. Here, we have extended the M2014 analysis up to early 2020 for a study region around Prudhoe Bay and Foggy Island Bay using a combination of sea ice charts from the National Ice Center (NIC) and the National Weather Service's Alaska Sea Ice Program (ASIP), together with our own analysis of open-access Sentinel-1 SAR imagery, which we refer to as the S1 dataset. Table 2 lists these data sources and the time spans they cover.

All four data sources are primarily dependent on satellite-based SAR imagery, but the analysis methods to identify landfast are not consistent. In the M2014 and S1 datasets, we followed a semi-automated approach first described by Mahoney et al. (2007). In short, this approach relies on the comparison of 3 consecutive images to identify sea ice that meets two criteria: i) ice is contiguous with the coast; and ii) ice lacks detectable motion over the period spanned by the 3 images. The time period for criterion (ii) depends on the availability of the satellite data used. In the M2014 dataset, this time period is approximately 20 days. In the S1 dataset, this time period is approximately 28 days, owing to the 14-day orbital period of the satellites. However, due to irregular availability of imagery over the study region, the dataset misses the freeze-up period in 2017 and the break-up period in all years except 2017.

The NIC and ASIP ice charts are compiled using the best available data at the time the chart is produced, which may include visible and thermal imagery when SAR data are not available. Such data allow the detection of open water at the edge of landfast ice (e.g., Fraser et al., 2012), but may not correctly identify the seaward edge of the landfast ice when there is no open water present. Additionally, analysts at NIC and ASIP may identify landfast ice based on appearance in SAR imagery in addition to, or instead of, any evidence of stationarity. The NIC ice charts are updated on a weekly basis, while the ASIP ice charts are updated daily from October 2015 onwards and on a weekly basis prior to that.

From each data source, we generated binarized raster images indicating the presence or absence of landfast ice within the study region at a resolution of 100 m. From these images, we determined the width of the landfast ice along a predefined set of coast-normal vectors (Fig. 4), following the approach of Mahoney et al. (2014). We then generated a time series capturing the annual cycle of the landfast advance and retreat along each vector for each year within our study period. In Fig. 4, the coast vectors in the neighborhood of the proposed Liberty Island site are highlighted in blue. For the purposes of the analysis that follows, we identified the calendar date each year when the average landfast ice width along these vectors extended beyond or retreated to within 10 km. This corresponds to the approximate distance of the Liberty Island site from shore and these dates therefore correspond to the first and last presence of landfast ice at the site.

Table 1
Deployment information for each SIMB deployed.

Year	Deployment date	Deployment location	Initial snow depth, m	Initial ice thickness, m	Recovery notes
2018	March 27	70.27432°N 147.58157°W	0.25	1.40	Satellite link lost on May 13
2019	February 2	70.27540°N 147.58697°W	0.03	1.04	Recovered by boat on June 24 after detachment of landfast ice

Table 2
Landfast ice extent data sources used in this study.

Data source	Time range
Mahoney et al., 2014 (M2014)	1996–2008
National Ice Center (NIC)	2000–2020
NWS Alaska Sea Ice Program (ASIP)	2007–2019
Sentinel-1 analysis (S1)	2016–2020

2.3. Single column model

Version 5 of the Los Alamos Sea Ice (CICE) model (Hunke et al., 2013) was used to simulate the seasonal changes of the ice thickness and snow depth from 1982 to 2019. The CICE model, designed for fully coupled global climate models, was run in standalone mode at one latitude/longitude location (at Liberty Island), with an idealized ocean mixed layer under sea ice. The CICE model was run on a single grid cell with 20 ice layers distributed across the ice thickness and one snow layer. The study location at Liberty (see Fig. 1) is shallow, with depths ranging from 3 to 5 m, and the simulations were initialized with the measured water depth and temperature, and salinity. The single column model was used and therefore had no ice dynamics. Mushy layer thermodynamics was used in the default setting. The CICE ocean mixed layer submodel uses fixed depth and only tracers (i.e. temperature and salinity) are updated through time by transport between the water and sea ice. The high vertical resolution provides a good representation of the steep salinity and temperature gradients near the top and bottom of the ice surface (Hunke, 2014). The model time step was 1 h. The CICE simulations were driven by meteorological input data (temperature, humidity, precipitation, winds, solar radiation, cloudiness, and surface pressure) from model output that will be described in later sections.

2.4. Meteorological observations and forecast data

Given the lack of in-situ meteorological observations in the vicinity of Liberty Island, this study made heavy use of atmospheric reanalysis data to provide baseline data for modeling ice growth with CICE. Reanalyses combine, in an optimal way, past short-term forecasts and observations to produce the most realistic state of the atmosphere. In this study we used the ERA5 reanalysis (Hersbach et al., 2020) which is produced by the European Centre for Medium-Range Weather Forecasts

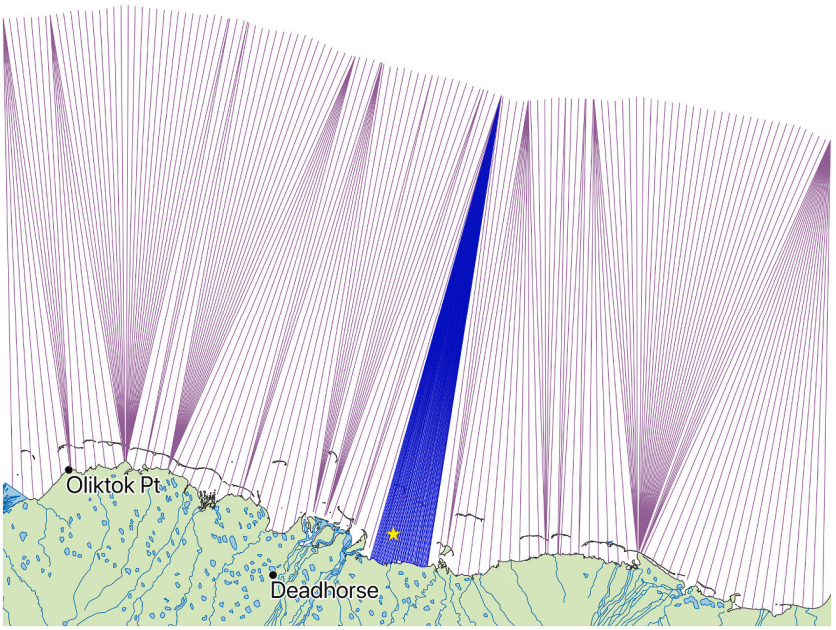

Fig. 4. The set of approximately coast-perpendicular vectors used to determine landfast ice width, with those representing Foggy Island Bay, shown in blue and the termination of the projected ice road indicated by a star. (For interpretation of the references to colour in this figure legend, the reader is referred to the web version of this article.)

(ECMWF). ERA5 is one of the newest state-of-the-art reanalysis products currently available and has shown good performance in the Arctic (Graham et al., 2019). It is a global data set that spans 1979-present with hourly time resolution and approximately 30 km grid spacing. For this analysis and running CICE we interpolated the required meteorological variables (described in the previous section) to the location of Liberty Island. Besides the SIMB field measurements described above, limited meteorological station data was obtained from the Snow Telemetry (SNOTEL) weather station at Prudhoe Bay and the Deadhorse airport weather station to help ground truth the reanalysis.

There are two major approaches to producing seasonal forecasts: statistical and dynamical. Statistical approaches often build regression, or similar, models based on past predictors to produce forecasts. Dynamical approaches use global climate models to simulate conditions in the coming months. This study evaluated the ability of a dynamical seasonal forecast model, in conjunction with CICE, to predict ice thickness at Liberty Island several months in advance. There are several modeling centers working in the area of seasonal prediction as it is a new and emerging field of forecasting. The Climate Forecast System (CFS) model version 2 is run by NOAA and provides operational seasonal predictions for the next 6–9 months (Saha et al., 2014). The CFS was selected for this study because it is the key seasonal forecast model used by NOAA and a member of the North American Multi-Model Ensemble (NMME) system (Kirtman et al., 2014). CFS includes a sea ice model, however landfast ice is not resolved/parameterized so the single column CICE model described in the previous section was employed in this study and driven by CFS meteorological outputs to simulate landfast sea ice thickness in the Foggy Island Bay. NOAA has produced a "hindcast" for CFS for 1982–2011 that is designed for the assessment of forecast skill. This hindcast is essentially a database of forecasts for past periods. The CFS also has an archive of operational forecasts since 2012 that now serve a similar purpose and were also analyzed. While several ensemble members were available from CFS for each forecast period, only the first ensemble member was used in our analysis for simplicity.

The meteorological input parameters from CFS and ERA5 were used to drive the CICE model described in the previous section. In all cases the CICE was run continuously over 1982–2019. One run was conducted using ERA5 to represent observed conditions and is directly compared against the field observations and ice chart/remote sensing products for model validation and calibration purposes. Two CFS forecast runs were also produced based on one CFS ensemble forecast each starting in September and running through February (forecasting the growth of ice) and a second run beginning in March and ending in August (capturing the melt season). Both runs branched off of the ERA5 data during the months preceding the start of the forecast period.

The accuracy of the ice thickness forecasts was primarily analyzed by standard metrics: the Root Mean Square Error (RMSE), Normalized RMSE (NRMSE) and skill score. The NRMSE metric normalized the root mean squared error of the CFS forecast to the ERA5 observed baseline as a percentage of the range of ERA5 results over the 1983–2018 period on each day. The mean square skill score used in this study was calculated as one minus the squared error of the forecast divided by that of a reference forecast. The reference forecast was the daily 1983–2018 long-term mean climatology produced by CICE using ERA5. So a skill value greater than zero indicates that the CFS forecast has less error than a simple forecast based on climatology. The Pearson's correlation coefficient was also used to assess the forecasts when applicable.

3. Results

3.1. Annual cycle of landfast ice extent in Foggy Island Bay

The 24-year record of landfast ice extent derived from satellite images and ice charts were used to quantify the typical extent of landfast in the region around Foggy Island Bay on a monthly basis (Fig. 5). This analysis shows that landfast ice typically forms at the location of the proposed Liberty Island site in November, although 10% of the time it was already present in October and in another 10% of years it did not form until December. At the other end of the annual cycle, our results indicate that landfast ice in Foggy Island Bay usually breaks-up in June. In 10% of years, it broke up in May, but it never persisted into July.

Combining all four datasets of landfast ice extent, we measured the seasonal variability in landfast ice width in Foggy Island Bay over the 24 annual cycles during the period 1996–2020 (Fig. 6). Apart from short-term variability during winter associated with the short-lived occurrences of "stable extensions" during which large areas of the Beaufort

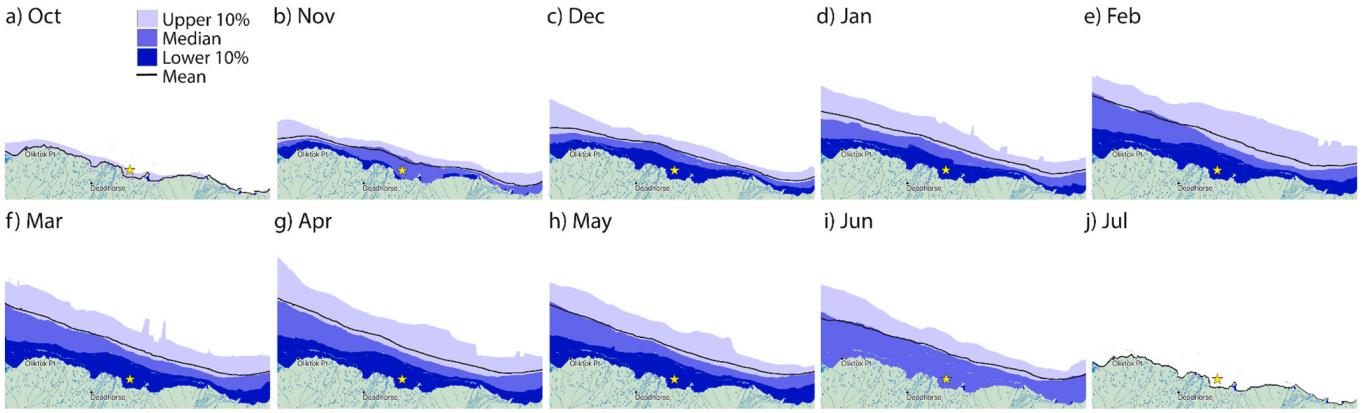

Fig. 5. Monthly landfast sea ice extent near Prudhoe and Foggy Island Bay based on remote-sensing data and ice charts for the time period 1996–2020. The colored areas indicate the lower 10%, median and upper 10% extents for each month, as indicated in the legend. The black lines indicate the mean extent. The yellow stars show the proposed location of the Liberty Island site. (For interpretation of the references to colour in this figure legend, the reader is referred to the web version of this article.)

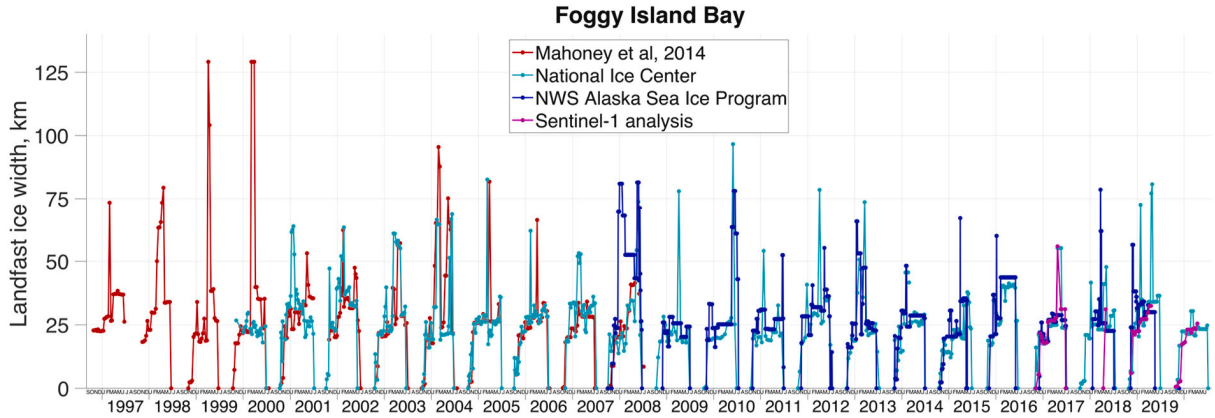

Fig. 6. Average landfast ice width for the period 1996–2020 determined from coast vectors illustrated in Fig. 10 using four different data sources.

Sea may be considered landfast (Mahoney et al., 2014), there is generally good agreement between the different data sources regarding the typical extent of landfast ice each year (Fig. 6).

Using a measured width $\geq$ 10 km to indicate the presence of ice at the proposed Liberty Island site, we calculated the annual date of "first landfast ice" and "last landfast ice" each year (Fig. 7). Close inspection of

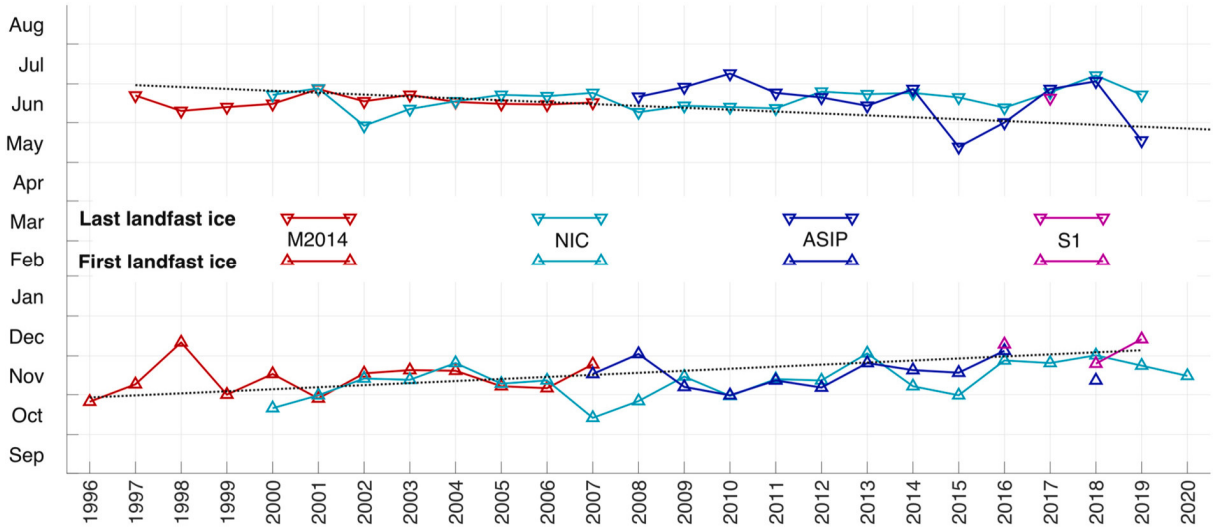

Fig. 7. First and last dates each year that landfast ice width in Foggy Island Bay exceeded 10 km, corresponding to the approximate location of Liberty Island. The two black dotted lines indicate linear regressions based on all data points. These trends are significant at >95%.

these data indicates that the landfast ice typically advances rapidly from the shoreline to approximately 20 km offshore within approximately 1 week of the first appearance of landfast ice at the coast (Fig. 6). The retreat of ice during breakup is similarly rapid. Thus, there appears to be no significant amount of time that the edge of the stable landfast is located near the Liberty Island location. However, the development of the island is likely to affect this situation and, while beyond the scope of this study, closer analysis of similar data in the vicinity of nearby Northstar Island may provide useful information regarding the potential effect of Liberty Island on surrounding landfast ice.

There was a 20-year period from 2000 to 2019 when we were able to compare landfast ice observations from multiple datasets. More often than not, the datasets agreed on the timing of first ice within 14 days and the timing of last ice to within 10 days. However, there were some notable exceptions. In 2015, for example, the last ASIP ice charts to show landfast ice at the Liberty Island location was on May 24, while the NIC charts continued to show landfast ice at this location until June 25. Also, in 2007, the only year when three datasets overlap, the M2014 and ASIP charts both showed first ice formation in mid to late November (November 25 and 17, respectively), while the NIC charts suggested landfast formation over a month earlier on October 14. Some of these differences arise from different reporting frequencies between datasets over time (e.g., in 2015, ASIP ice charts are available on a daily basis, while NIC charts were produced weekly), but we assume that different practices between individual analysts must also contribute.

Combining dates from all data sources with equal weight, we find significant linear trends (at >95% level) in both later formation and earlier retreat of landfast ice at the proposed Liberty Island site. Overall, from 1996 to 2020, we find that landfast ice is forming 1.6 days later ($R^2 = 0.15$, $p = 0.006$) and breaking-up 1.5 days earlier ($R^2 = 0.11$, $p = 0.016$) per year, on average.

3.2. Ice mass-balance observations

The ice thickness, snow depth and the through-ice temperature profile recorded by the SIMBs captured a number of important seasonal events in 2018 and 2019 (Fig. 8). The deployment in 2018 resulted in only 46 days of data, during which time the ice thickened from 1.40 m to 1.51 m. The record ends just after the snow pack had warmed to the melting point, representing the earliest stage of the melt season (Fig. 8a). The maximum ice thickness measured was therefore likely close to the maximum thickness achieved in 2019.

The SIMB deployed in 2019 recorded 142 days of data, during which time the ice reached a maximum ice thickness of 1.53 m and a maximum snow depth of 0.25 m (Fig. 8b). The majority of the snow fell during a single event around March 14, after which time cold temperatures ceased penetrating the ice underneath, which remained above −10 °C. The maximum ice thickness was achieved May 21, shortly after the snow pack began thinning and coinciding with the arrival of warm water below the ice. Bottom melt began around May 26, but short-lived episodes of apparent rapid bottom growth suggest the formation of "false bottoms" (Notz et al., 2003), which may have masked an earlier onset of

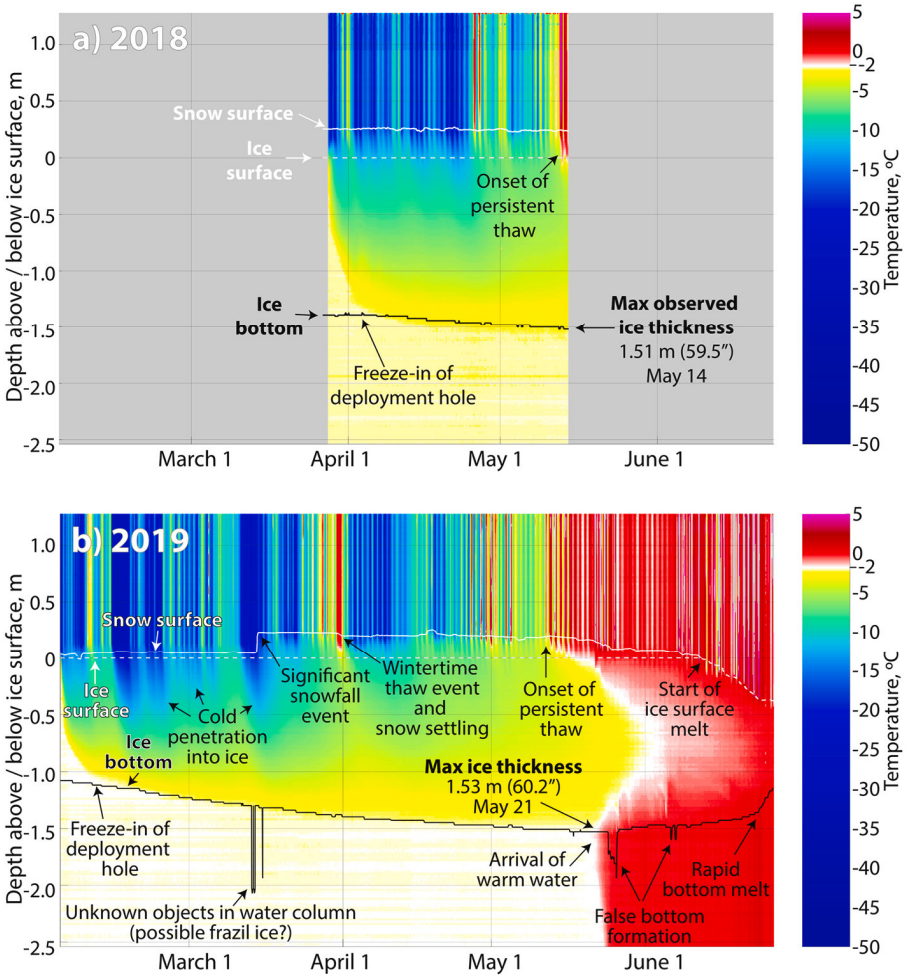

Fig. 8. SIMB measurements from a) 2018, and b) 2019. Solid white lines show snow depth, while dashed white lines show the position of the ice surface. Solid black lines show the position of the ice bottom. The colour scale illustrates the variation of the air-snow-ice-ocean temperature profile over time.

bottom melt. The snow at the SIMB completely melted June 13, marking the onset of surface ice melt. In total, the ice around the SIMB thinned by 0.55 m before the buoy was recovered. Ablation included 0.19 m of bottom melt and 0.36 m of melt at the top of the ice. A marked increase in bottom melt on June 24 coincided with the detachment of landfast ice in which the SIMB had been deployed. The buoy was recovered 3 days later by boat.

3.3. Modeling observed ice thickness

To place the ERA5 data in the context of local station data, key variables of temperature, precipitation and cloud cover were evaluated against the limited weather station data record at Prudhoe Bay and Deadhorse (Fig. 9). Temperature compares well with the SNOTEL weather station at Prudhoe Bay with ERA5 being around 2–3 °C warmer in winter on average and 1–3 °C cooler in summer in 2004–2018. The ERA5 precipitation had larger deviations from the SNOTEL station with a wet bias approaching 7 mm in August. The reanalysis is also significantly cloudier than the observations at the Deadhorse airport. The ERA5 mean cloudiness exceeded 70% in all months with the cloudiest months in winter while the station indicated the maximum cloudiness in May–October. These deviations from the available observations will be considered as we interpret the results of the analysis in later sections.

The CICE model was run over the period of record driven by the inputs from the ERA5 reanalysis. This simulation provides the best estimate of observed ice thickness at Liberty Island in the absence of in-situ measurements. The results of this "observed" reanalysis simulation are compared with the field measurements of ice thickness and snow depth from the SIMB in winters 2017–18 and 2018–19 in Fig. 10. The 2017–18 season had very limited SIMB data but the ice thickness and snow depth were broadly similar during April, when observations were available in both winters. The ice thickness in CICE captured the observed values quite well in February–June 2019 but was delayed in the timing of melt in July. The timing of the onset of snowmelt was well captured in 2019. The snow depth estimated from ERA5 in CICE built up more gradually than the sharp increases observed at the site in February and March 2019, however both reached similar end-of-season snow depth. Abrupt increases in snow depth measured by the SIMB coincided with storm events, indicating that snow accumulation is sensitive to the occurrence of such events. Additionally, some care is needed when interpreting these short increases in snow depth, since storms do not typically distribute snow evenly on sea ice, with snow collecting instead in dunes and drifts. Given the importance of snow for insulating the ice and slowing ice growth in winter, it may be advisable to deploy additional sensors to better assess variability of snow depth at the site. While beyond the scope of this study, further analysis should directly examine the sensitivity of forecast skill to snow. One example of such future analysis or application might consider different perturbations of the snowpack that could be used to create an ensemble prediction with CICE.

3.4. Seasonal forecasting

The meteorological parameters used to drive CICE from CFS were first compared with those of the ERA5 reanalysis over the hindcast period to identify possible areas of uncertainty (Fig. 11). The CFS was generally warmer than ERA5 in the summer and early winter. This matches the enhanced solar radiation in CFS over the same seasons. The precipitation was quite comparable between the two data sets.

The CFS had generally weaker winds throughout much of the year but best matches the ERA5 July–November. Atmospheric moisture is generally comparable, but cloudiness in CFS was significantly reduced relative to ERA5. In the previous section it was found that the observed cloudiness at Deadhorse was also much lower than what is found in ERA5, therefore CFS actually may have more reasonable cloudiness on average than the reanalysis at Liberty Island. Based on these findings

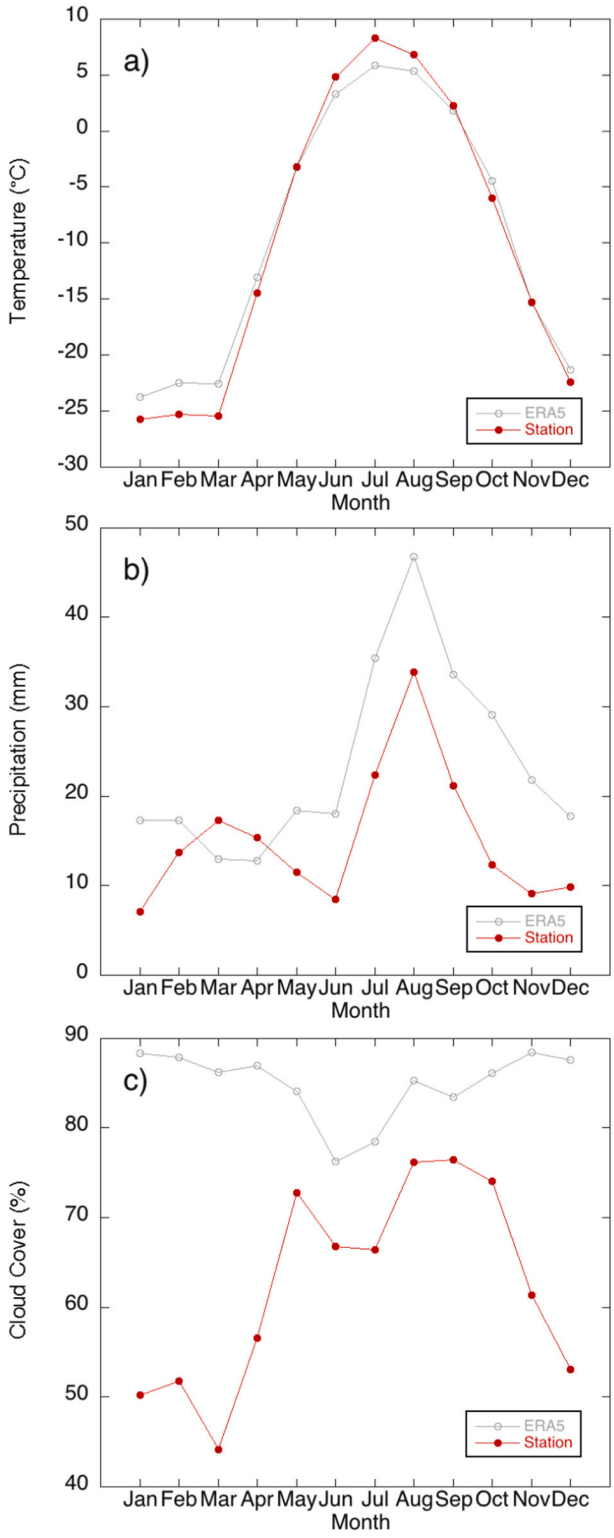

Fig. 9. Monthly ERA5 reanalysis (gray) and weather station (red) 2004–2018 climatologies of temperature (a; °C), precipitation (b; mm), and cloud cover (c; %). (For interpretation of the references to colour in this figure legend, the reader is referred to the web version of this article.)

hypothetical bias corrections were prepared for all variables. This correction was a simple adjustment of the values based on the long-term mean difference for each period and was performed for demonstration purposes. The results of the CICE shown in the rest of this section do not include such an adjustment of the forcing data but consider bias

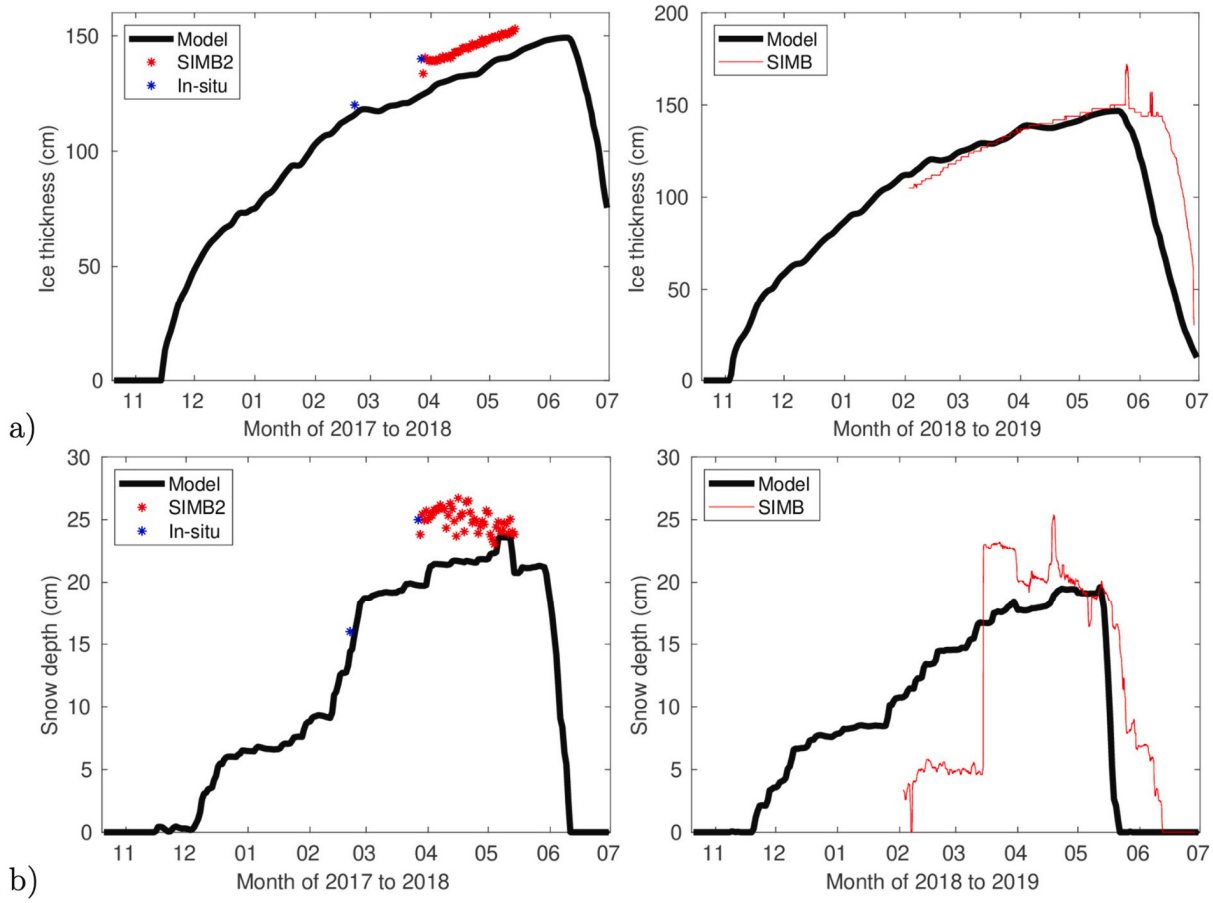

Fig. 10. CICE simulations of ice thickness (top row) and snow depth (bottom row) for winter 2017–18 (left) and 2018–19 (right). The model simulations were driven by the ERA5 reanalysis and are displayed as black lines, while the SIMB measurements are shown in red and direct measurement by personnel are in blue. The units of all parameters are cm. (For interpretation of the references to colour in this figure legend, the reader is referred to the web version of this article.)

adjustments of the output ice thickness.

Two forecast periods were the focus of the evaluation of CFS: September–February to capture onset and establishment of sea ice; and March–August to forecast the onset of melt. Additional forecast periods are available from CFS and could be considered in an operational setting. The CICE model was run over 1983–2019 separately for each period with the ERA5 used to provide realistic conditions outside of the forecast period. This procedure produced one September–February ice thickness forecast each year and one similar for March–August for evaluation. Since ice thickness measurements were not available outside of 2018–19 the forecast evaluation used the ERA5 reanalysis CICE simulation as the baseline. An assessment of the daily average 1983–2018 CFS vs. ERA5 CICE ice thickness revealed a general bias toward lower ice thickness, later ice formation onset, and earlier ice free conditions when using the CFS forcing data (not shown). Due to these biases, a simple correction was applied to the forecast ice thickness by adding difference of the long-term means to the daily forecast ice thickness (i.e. a delta method). The results of the bias-corrected forecasts for predicting daily sea ice thickness, their mean error relative to the ERA5 estimates and skill scores are shown in Fig. 12. Introducing bias-correction improves forecast skill throughout the year. In fact, skillful seasonal forecasts would not be possible without bias correction (Fig. 12b). The greatest error is during the time of onset but declines as the ice becomes stable. For instance, the error in the forecast initialized in March is relatively small while ice is stable in the winter but increases during the melt season when conditions become more variable. Forecast skill was greatest for the September forecasts during the early months of the ice formation/growth season and then declined in December and January. The forecast skill is very high for the March forecast period when the ice thickness is most stable in March–May but declines quickly before rebounding in July. This indicates that it is difficult for the March forecasts to capture the timing of onset of melt. Likewise, the seasonal forecasts of maximum ice thickness produced in September are highly uncertain.

The forecasts were evaluated in the context of the ice chart/remote sensing-based data described earlier (Fig. 13). The September–February freeze-up date forecasts and ERA5 simulation (when the CICE modeled ice thickness first exceeded 1 cm) were compared with the ice chart/remote-sensing first landfast ice dates. The reanalysis captures much of the observed variability of the first landfast ice dates with a correlation of 0.56, while the forecast has an expectedly weaker correlation with observations at 0.07. The date of breakup or last ice (when the CICE modeled ice thickness fell below 90 cm) is less consistent with both modeled reanalysis and the test forecasts with correlations of −0.01 and 0.13, respectively. Some deviation is expected since the remote sensing products are purely based on the presence/absence of ice in the vicinity of Liberty Island within 10 km of the coast while the CICE modeled dates were based on reaching specific ice thickness thresholds.

A targeted evaluation of the forecasts of ice thickness thresholds outlined in Fig. 3 are needed, but in the absence of an observed record ERA5 was used as the baseline for comparison. The first and last date reaching specific ice thresholds were compared relative to the mean date (see mean dates in Table 3) for ease of comparison (Fig. 14). The CFS forecast RMSEs and skill scores for the threshold dates are shown in Table 3. The first date of 82 cm and 133 cm have the greatest year to year variability and have skill scores of 0.12 and − 0.39, respectively. The

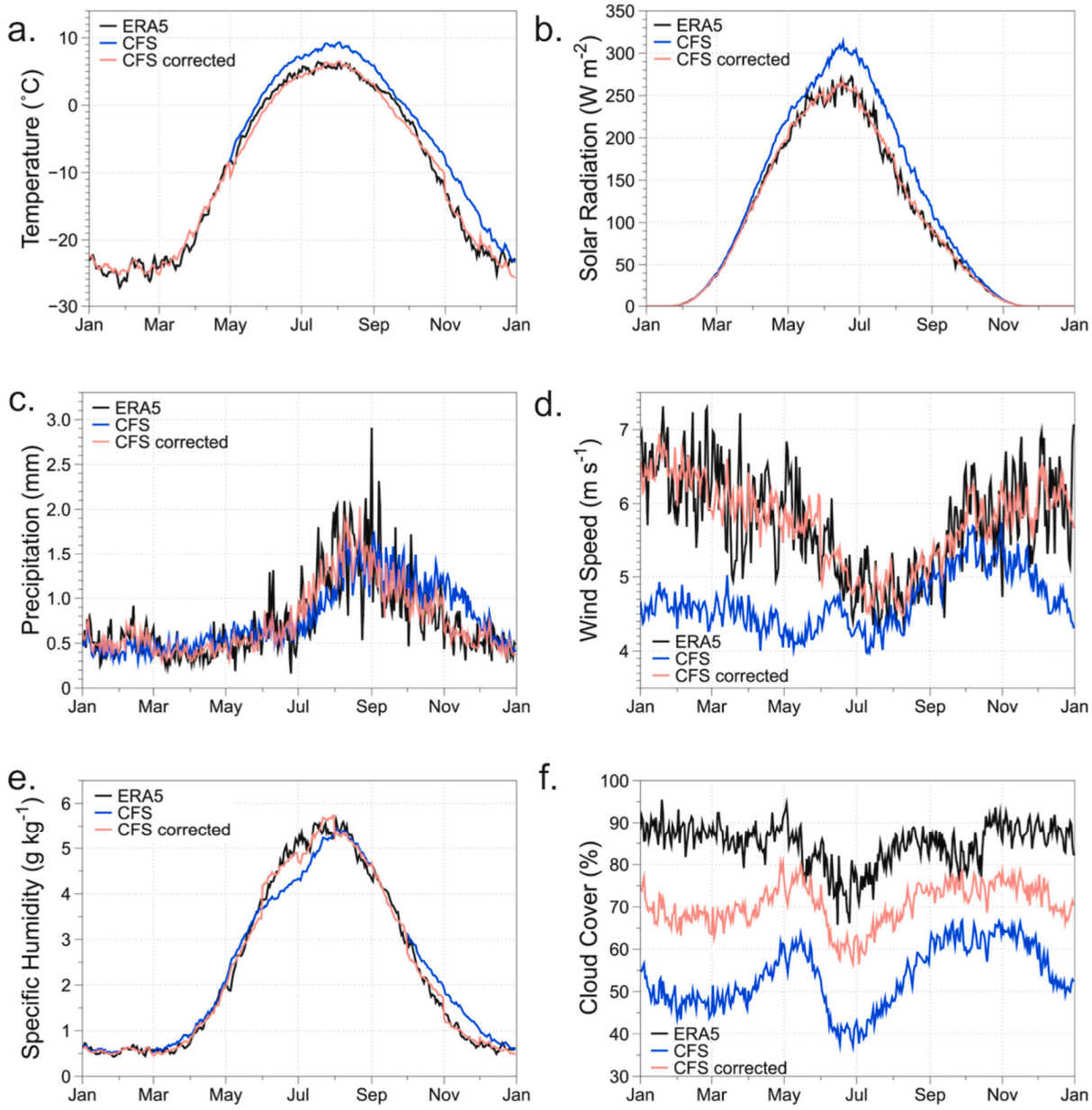

Fig. 11. CFS and ERA5 1982–2011 daily climatologies with hypothetical bias corrections for CFS for key input variables for CICE.

best predicted threshold date was the first 51 cm and that has a skill score of 0.50. Skill scores were negative for the remaining threshold date forecasts.

4. Discussion

Planning for safe and efficient offshore operations in the Arctic requires forecasts of relevant ice properties that are both skillful and seasonal in range. Prior work has shown that melt-driven breakup of landfast ice in northern Alaska can be accurately predicted 1–2 weeks in advance (Petrich et al., 2012), but this is too short-term to be useful for seasonal planning. The present study attempts to greatly expand the forecast window out to several months in advance, while maintaining as much forecast skill as possible. At broader spatial scales the CFS, considered in our evaluation, has shown predictive skill in seasonal-scale forecasts of Arctic sea ice concentration/extent (Liu et al., 2018; Merryfield et al., 2013). However, the CFS model does not resolve landfast ice on its own and therefore this study utilized a standalone single column CICE model to better capture the landfast ice conditions at Liberty Island. The CICE forecasts driven by the CFS were generally challenged with low predictive skill scores with the exception of the onset dates in November–December and the final melt out in July. Bias correction of the seasonal forecasts was found to be a necessary step to build forecast skill into those periods. Similar challenges have been identified more broadly for seasonal forecasting of the Arctic sea ice extent and concentrations (Zhao et al., 2020; Blanchard-Wrigglesworth et al., 2017). Bias corrections have also led to improvements in other Alaska seasonal forecasting applications of CFS related to wildfire danger ratings (Sampath et al., 2021). In this study, the CICE hindcasts/forecasts over 1983–2019 were biased toward later onset of ice and earlier breakup dates. The bias correction during the start and end of the season therefore had the effect of bringing the forecasts much closer to climatology. This adjustment had a relatively large impact on the skill during these periods and was responsible for the rebound of skill in June–July in the March–August forecasts.

Potential sources of seasonal-scale predictability of landfast ice

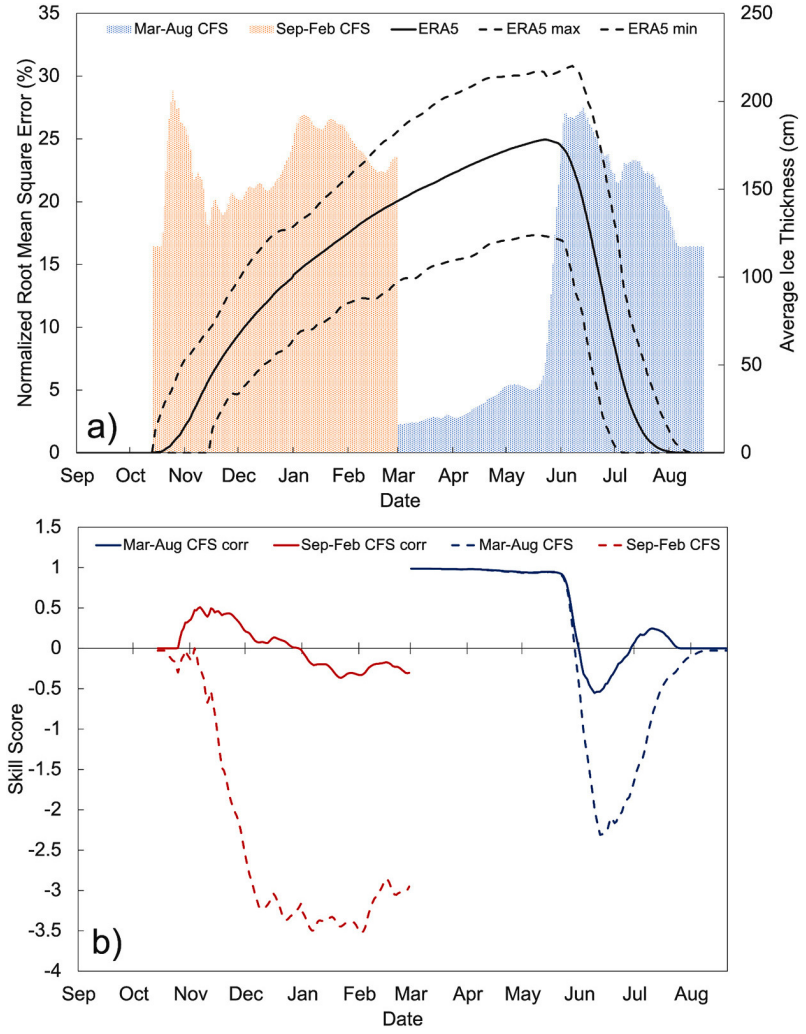

Fig. 12. CFS hindcast ice thickness (a) Normalized Root Mean Square Error (shading) relative to ERA5 climatological average and overall max/min ice thickness (black lines), and (b) mean square error skill scores for the hindcast with (solid lines) and without (dashed lines) bias corrections.

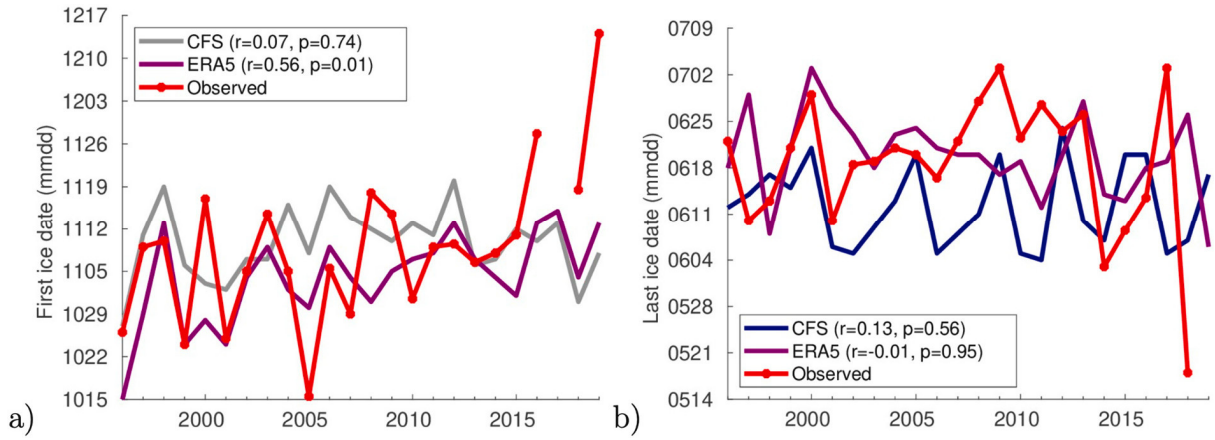

Fig. 13. Observed, ERA5, and forecast date of freeze-up/first landfast ice (a) and last date of landfast ice (b). The date of freeze-up/first ice is defined as the date with first ice thickness >1 cm and the last date is the date <90 cm. The correlation (r) and statistical significance of the correlations (*p*) with the observations are shown for the CFS forecast and ERA5 reanalysis in the legends.

thickness may come from teleconnections such as the El Niño Southern Oscillation (ENSO) and the Pacific Decadal Oscillation (PDO). While the links between teleconnection indices and landfast ice in the region have not been established, ENSO and PDO have each been tied with monthly and seasonal-scale variability in near-surface air temperature throughout the Alaska region (Papineau, 2001; Hartmann and Wendler,

Table 3
Average dates of key ice thickness threshold exceedance in ERA5 CICE 1983–2019 simulation and RMSE, and skill score metrics for CFS forecast vs. ERA5.

Parameter	Average date	RMSE	Reference RMSE	Skill score
First 51 cm	November 20	10	14	0.50
Last 51 cm	July 2	8	7	−0.35
First 82 cm	December 16	18	19	0.12
Last 82 cm	June 26	8	7	−0.28
First 133 cm	February 13	36	31	−0.39
Last 133 cm	June 13	9	7	−0.72

The Reference RMSE is for a forecast based on the long-term ERA5 climatology (average date). The units of the RMSEs are in days.

2005; Bieniek et al., 2014; Bieniek et al., 2011). Sea ice in the Beaufort Sea region has more broadly been linked with the PDO, ENSO, and other North Pacific teleconnection patterns (Clancy et al., 2021; Kim et al., 2020; Yang et al., 2020; Zhang et al., 2019) and the Arctic Oscillation (Armitage et al., 2018; Stroeve et al., 2011; Liu et al., 2004; Rigor et al., 2002). The PDO also influences sea ice variability in the nearby Bering Sea (Zhang et al., 2010). Specialized analysis of the large-scale atmospheric drivers beyond the scope of this study would be needed to identify the physical mechanisms that link such teleconnections with the seasonal predictability of landfast ice in the Foggy Island Bay region. This is a priority topic for future research to advance understanding predictability of landfast ice in Alaska.

The magnitude of the targeted uncertainty or the desired prediction skill has been loosely defined by the operator as an interval of +/− 1 week around the observed date allowing for start of on-ice operations. This compares to a much larger window of uncertainty of +/− 4–6 weeks associated with present practice that draws on climatology and proprietary operator data (J. Gardner, personal communication, 2020). The RMSEs for the onset and final dates for all key thresholds based on the CICE/CFS forecasts, except for the first 133 cm, are within +/− 8–18 days. While still outside the desired one-week window, this is a substantial reduction of the uncertainty associated with current practice. Nevertheless, the CFS model forecasts still lag the forecasts from climatology for many parameters. As noted in the previous paragraph, these error estimates are not based on in-situ observations such that additional uncertainties still exist. Considering this latter circumstance, there is great value in increasing the number of observations of landfast ice formation, growth, decay, and breakup at the specific study location. While SAR data have both temporal and spatial resolution sufficient to capture freeze-up and break-up processes (see Fig. 6), a larger number of time series of ice thickness from the point of landfast ice formation through its decay and break-up are needed to improve model performance in the prediction system. Of particular value in this context are the following:

(1) Data on the time lag between freeze-up and formation of landfast ice. Freeze-up is the annual event predicted by the CICE/CFS forecast, while landfast ice formation is the annual event captured by satellite data and ice charts and is most relevant to offshore operators. The lag between these events can add significant uncertainty also in the seasonal scale prediction. This lag has a thermal component (i.e. residual ocean heat that retards sea ice growth even after freeze-up) and a dynamic component, (i.e., the prevention of landfast ice attachment or anchoring by strong winds, currents, or waves). Moreover, the first landfast ice that does eventually form may be in the form of advected new or first-year ice which can lead to faster attainment of required load-bearing capacity. However, it is unclear as to how common this process is at the study site.
(2) Time series data of snow depth on sea ice. Snow depth has a first order effect on ice growth. Snow depth on sea ice can also be highly variable at small scales (e.g. Nicolaus et al., 2021) and so multiple measurements at each forecast location would be ideal.
(3) Ice growth and ice melt rate data in the early and late stages of landfast ice season when a number of factors, including ocean-to-ice heat fluxes, can increase model errors and uncertainties. If such data are not available, then information on upper ocean heat content and derived ocean-to-ice heat fluxes would be of value.

Testing of an ensemble approach to prediction, while beyond the scope of this study, might help to improve the forecasts since multi-model ensembles can outperform the seasonal forecasting skill of individual members (e.g. Kirtman et al., 2014; Merryfield et al., 2013; Palmer et al., 2004). This study used the single column CICE model to produce the ice thickness parameters based on CFS and ERA5 meteorological forcing data; however, other models or configurations could

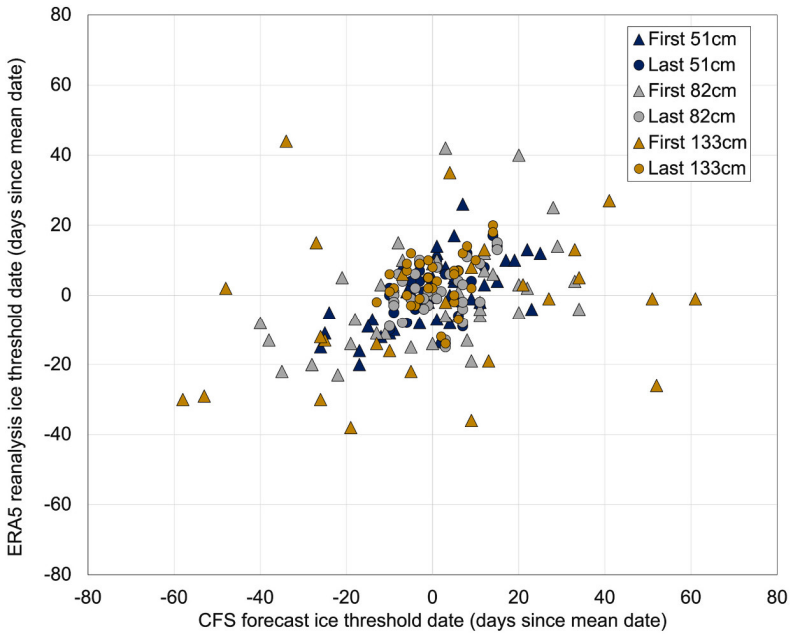

Fig. 14. CICE CFS forecast vs. ERA5 reanalysis dates of key ice thickness thresholds relative to their mean date. Mean dates for ERA5 are given in Table 3.

also be considered. These include regional ocean modeling with ice thickness-based parameterizations of landfast ice attachment (e.g., Lemieux et al., 2015) or more simple degree day models. Besides seasonal forecasting with dynamical models, statistical forecasting approaches, such as analogs, also show promising results in the region (Walsh et al., 2021) and could be an additional method to forecast landfast ice. However, in any approach a major source of uncertainty comes from the lack of long-term observations, in this case, near Liberty Island. Observations on ice thickness are especially important as they are needed to calibrate and validate the forecasts. This study only had limited direct field observations of ice thickness that did not capture the full seasonal cycle and had to rely heavily on modeled estimates produced using atmospheric reanalysis forcing data. Expanded long-term observations of ice thickness in the region would be necessary to better evaluate forecast skill in a way that is most meaningful for operators who would build ice roads, etc.

5. Conclusions

This study implemented a scheme for seasonally forecasting the thickness of sea ice in the landfast ice zone of Foggy Island Bay for the purposes of planning offshore development activities. The location chosen for this study was the proposed Liberty gravel island site in northern Alaska. Our approach relied on the single column ice growth model, CICE in single column mode, forced by seasonal atmospheric forecast data from CFS. Results were validated against limited observational data from a SIMB deployed near the study location in 2018–19 and 2019–20 as well as satellite and ice chart observations of landfast ice extent. Comparison with ERA5-forced CICE results was necessary for bias correction. The integration of multiple products was necessary due to the lack of long-term in-situ observations in the region and the absence of seasonal forecasting models that resolve landfast ice. Modest forecast skill relative to forecasts from climatology was possible during the early season and later in the melt season (using atmospheric forcing data from the CFS initialized in August and March, respectively). Bias correction of the forecasts was valuable and necessary to improve the skill. Skill was highest in mid-winter once the ice was fully established.

Forecast skill for capturing the timing of reaching specific ice thickness thresholds for ice trafficability was mixed. The best skill was in forecasting the initial dates of landfast ice formation and forecasts based on ERA5 long-term climatology outperformed those based on CFS for the end-of-season thresholds. However, in all cases forecasts for these thresholds were better constrained than the current forecasting approaches typically used by industry. A major source of uncertainty for the evaluation of the seasonal forecasts in this region is the lack of in-situ observations of sea ice thickness and snow depth. Additional long-term observations will be necessary to better assess and calibrate forecasts in the future for operational use. Combining observations of landfast ice extent from all data sources, we find significant linear trends (at >95% level) in the start and end of the annual cycle, with landfast ice at the study site forming 1.6 days later and breaking up 1.5 days earlier each year, on average.This is in line with larger-scale trends in landfast ice seasonality (Mahoney et al., 2014) and freeze-up/break-up of coastal ice in northern Alaska (Johnson and Eicken, 2016). This is relevant from an operational perspective and likely implies a corresponding ice thickness trend toward thinner ice.

Because of lack of suitable data to constrain model boundary conditions, the current study assumed that ice growth proceeds with natural snow build-up. From an ice management perspective, snow removal and flooding of sections of ice for ice road build-up would increase the length of the operating season. Such snow and ice management may also increase predictive skill of the long-range forecast through the removal of uncertainties associated with major snowfall events (such as those shown in Figs. 8 and 10) and greater variability in snow depth and thermal properties. Such management approaches are commonly employed by industry (BP and Golder Associates, 2013; Bashaw et al., 2013) and could be incorporated into the ice growth model and prediction system.

The specific processes that are critical in terminating on-ice operations (e.g., onset of surface melt ponding or melt-out of wide cracks, see Fig. 3) require further study. Both, active ice management and assessment of ice mechanical properties relevant to bearing strength may improve prediction through clearer delineation of the operations window, and may build on the finding of greater predictive skill toward the end of the ice season (Fig. 12). Such work would also provide better bounds on the predictand variable for end of on-ice operations, which is currently taken to be either a simple ice thickness or temperature threshold.

CRediT authorship contribution statement

Peter A. Bieniek: Conceptualization, Methodology, Formal analysis, Visualization, Project administration, Funding acquisition, Writing - original draft, Writing - review & editing. **Hajo Eicken:** Conceptualization, Methodology, Funding acquisition, Writing - original draft, Writing - review & editing. **Meibing Jin:** Formal analysis, Validation, Investigation, Writing - original draft. **Andrew R. Mahoney:** Methodology, Formal analysis, Visualization, Writing - original draft. **Josh Jones:** Investigation, Visualization, Data curation, Writing - original draft. **Uma S. Bhatt:** Visualization, Writing - review & editing.

Declaration of Competing Interest

The authors have no competing interests to declare.

Acknowledgements

The authors thank Jennifer Gardner for her crucial guidance that led to the success of this project and Kate Kaufman, James Jackson, Mark Barbham, David Deitzgen, and Charles McNall for their technical or logistical support with the field work. We also thank the two reviewers for their fruitful comments that helped to improve this manuscript. This study was funded by Hilcorp Alaska LLC. Additional funding support for M. Jin was provided by National Science Foundation Office of Polar Programs Grant 1735862.

References

Armitage, T.W.K., Bacon, S., Kwok, R., 2018. Arctic sea level and surface circulation response to the Arctic Oscillation. Geophys. Res. Lett. 45, 6576–6584. https://doi.org/10.1029/2018GL078386.

Bashaw, E.K., Drage, J., Lewis, S.K., Billings, C.J., 2013. Applied ice engineering for exploring Arctic natural resources. In: ISCORD 2013: Planning for sustainable cold regions, pp. 308–319.

Bieniek, P.A., Bhatt, U.S., Rundquist, L.A., Lindsey, S.D., Zhang, X., Thoman, R.L., 2011. Large-scale climate controls of interior Alaska river ice breakup. J. Clim. 24, 286–297. https://doi.org/10.1175/2010JCLI3809.1.

Bieniek, P.A., Walsh, J.E., Thoman, R.L., Bhatt, U.S., 2014. Using climate divisions to analyze variations and trends in Alaska temperature and precipitation. J. Clim. 27, 2800–2818. https://doi.org/10.1175/JCLI-D-13-00342.1.

Blanchard-Wrigglesworth, E., Barthélemy, A., Chevallier, M., Cullather, R., Fučkar, N., Massonnet, F., Posey, P., Wang, W., Zhang, J., Ardilouze, C., Bitz, C.M., Vernieres, G., Wallcraft, A., Wang, M., 2017. Multi-model seasonal forecast of Arctic Sea-ice: forecast uncertainty at pan-Arctic and regional scales. Clim. Dyn. 49, 1399–1410. https://doi.org/10.1007/s00382-016-3388-9.

BP & Golder Associates, 2013. Best Management Practices for Building and Working Safely on Ice Roads. Anchorage, Alaska, 81pp.

Bushuk, M., Msadek, R., Winton, M., Vecchi, G., Yang, X., Rosati, A., Gudgel, R., 2019. Regional Arctic Sea–ice prediction: potential versus operational seasonal forecast skill. Clim. Dyn. 52, 2721–2743. https://doi.org/10.1007/s00382-018-4288-y.

Clancy, R., Bitz, C., Blanchard-Wrigglesworth, E., 2021. The influence of ENSO on Arctic Sea Ice in large ensembles and observations. J. Clim. 34, 9585–9604. https://doi.org/10.1175/JCLI-D-20-0958.1.

Dammann, D.O., Eriksson, L.E.B., Mahoney, A.R., Eicken, H., Meyer, F.J., 2019. Mapping pan-Arctic landfast sea ice stability using Sentinel-1 interferometry. Cryosphere 13 (2), 557–577. https://doi.org/10.5194/tc-13-557-2019.

Dumas, J., Carmack, E., Melling, H., 2005. Climate change impacts on the Beaufort shelf landfast ice. Cold Reg. Sci. Technol. 42, 41–51.

Eicken, H., Lovecraft, A.L., Druckenmiller, M., 2009. Sea-ice system services: a framework to help identify and meet information needs relevant for Arctic observing networks. Arctic 62 (2), 119–136.

Ford, J.D., Clark, D., Pearce, T., Berrang-Ford, L., Copland, L., Dawson, J., Harper, S.L., 2019. Changing access to ice, land and water in Arctic communities. Nat. Clim. Chang. 9 (4), 335–339. https://doi.org/10.1038/s41558-019-0435-7.

Fraser, A.D., Massom, R.A., Michael, K.J., Galton-Fenzi, B.K., Lieser, J.L., 2012. East Antarctic landfast sea ice distribution and variability, 2000–08. J. Clim. 25 (4), 1137–1156.

Graham, R.M., Hudson, S.R., Maturilli, M., 2019. Improved performance of ERA5 in Arctic gateway relative to four global atmospheric reanalyses. Geophys. Res. Lett. 46, 6138–6147.

Hartmann, B., Wendler, G., 2005. The significance of the 1976 Pacific climate shift in the climatology of Alaska. J. Clim. 18, 4824–4839.

Hersbach, H., Bell, B., Berrisford, P., Hirahara, S., Horányi, A., Muñoz-Sabater, J., Nicolas, J., Peubey, C., Radu, R., Schepers, D., Simmons, A., Soci, C., Abdalla, S., Abellan, X., Balsamo, G., Bechtold, P., Biavati, G., Bidlot, J., Bonavita, M., De Chiara, G., Dahlgren, P., Dee, D., Diamantakis, M., Dragani, R., Flemming, J., Forbes, R., Fuentes, M., Geer, A., Haimberger, L., Healy, S., Hogan, R.J., Hólm, E., Janisková, M., Keeley, S., Laloyaux, P., Lopez, P., Lupu, C., Radnoti, G., de Rosnay, P., Rozum, I., Vamborg, F., Villaume, S., Thépaut, J.N., 2020. The ERA5 global reanalysis. Q. J. R. Meteorol. Soc. 146, 1999–2049. https://doi.org/10.1002/qj.3803.

Hunke, E.C., 2014. Sea ice volume and age: Sensitivity to physical parameterizations and thickness resolution in the CICE Sea ice model. Ocean Model 82, 45–59. https://doi.org/10.1016/j.ocemod.2014.08.001.

Hunke, E.C., Lipscomb, W.H., Turner, A.K., Jeffery, N., Elliott, S., 2013. CICE: The Los Alamos Sea Ice Model Documentation and Software User's Manual LA-CC-06-012.

Johnson, M., Eicken, H., 2016. Estimating Arctic Sea-ice freeze-up and break-up from the satellite record: a comparison of different approaches in the Chukchi and Beaufort Seas. Elementa: Sci. Anthropocene 4, 000124. https://doi.org/10.12952/journal.elementa.000124.

Kim, H., Yeh, S.W., An, S. Il, Song, S.Y., 2020. Changes in the role of Pacific decadal oscillation on sea ice extent variability across the mid-1990s. Sci. Rep. 10, 1–10. https://doi.org/10.1038/s41598-020-74260-0.

Kirtman, B.P., Min, D., Infanti, J.M., Kinter, J.L., Paolino, D.A., Zhang, Q., van den Dool, H., Saha, S., Mendez, M.P., Becker, E., Peng, P., Tripp, P., Huang, J., DeWitt, D. G., Tippett, M.K., Barnston, A.G., Li, S., Rosati, A., Schubert, S.D., Rienecker, M., Suarez, M., Li, Z.E., Marshak, J., Lim, Y.-K., Tribbia, J., Pegion, K., Merryfield, W.J., Denis, B., Wood, E.F., 2014. The North American Multimodel Ensemble: phase-1 seasonal-to-interannual prediction; phase-2 toward developing intraseasonal prediction. Bull. Am. Meteorol. Soc. 95, 585–601. https://doi.org/10.1175/bams-d-12-00050.1.

Lemieux, J.F., Tremblay, L.B., Dupont, F., Plante, M., Smith, G.C., Dumont, D., 2015. A basal stress parameterization for modeling landfast ice. J. Geophys. Res. Ocean. 120, 3157–3173. https://doi.org/10.1002/2014JC010678.

Lemieux, J.F., Dupont, F., Blain, P., Roy, F., Smith, G.C., Flato, G.M., 2016. Improving the simulation of landfast ice by combining tensile strength and a parameterization for grounded ridges. J. Geophys. Res. Oceans 121 (10), 7354–7368.

Liu, J., Curry, J.A., Hu, Y., 2004. Recent Arctic Sea ice variability: connections to the Arctic Oscillation and the ENSO. Geophys. Res. Lett. 31, 9211. https://doi.org/10.1029/2004GL019858.

Liu, Y., Wang, W., Kumar, A., 2018. Multiweek prediction skill assessment of arctic sea ice variability in the CFSv2. Weather Forecast. 33, 1453–1476. https://doi.org/10.1175/WAF-D-18-0046.1.

Mahoney, A., Eicken, H., Gaylord, A.G., Shapiro, L., 2007. Alaska landfast sea ice: links with bathymetry and atmospheric circulation. J. Geophys. Res. Oceans 112 (C2), C02001. https://doi.org/10.1029/2006JC003559.

Mahoney, A.R., Eicken, H., Gaylord, A.G., Gens, R., 2014. Landfast Sea ice extent in the Chukchi and Beaufort Seas: the annual cycle and decadal variability. Cold Reg. Sci. Technol. 103, 41–56.

Mäkynen, M., Karvonen, J., Cheng, B., Hiltunen, M., Eriksson, P.B., 2020. Operational service for mapping the Baltic Sea landfast ice properties. Remote Sens. 12, 4032.

Merryfield, W.J., Lee, W.S., Wang, W., Chen, M., Kumar, A., 2013. Multi-system seasonal predictions of Arctic Sea ice. Geophys. Res. Lett. 40, 1551–1556. https://doi.org/10.1002/grl.50317.

Nicolaus, M., et al., 2021. Snow depth and air temperature seasonality on sea ice derived from snow buoy measurements. Front. Mar. Sci. 8 (377) https://doi.org/10.3389/fmars.2021.655446.

Notz, D., McPhee, M.G., Worster, M.G., Maykut, G.A., Schlunzen, K.H., Eicken, H., 2003. Impact of underwater-ice evolution on Arctic summer sea ice. J. Geophys. Res. Oceans 108 (C7). https://doi.org/10.1029/2001jc001173.

Palmer, T.N., Alessandri, A., Andersen, U., Cantelaube, P., Davey, M., Délécluse, P., Déqué, M., Díez, E., Doblas-Reyes, F.J., Feddersen, H., Graham, R., Gualdi, S., Guérémy, J.-F., Hagedorn, R., Hoshen, M., Keenlyside, N., Latif, M., Lazar, A., Maisonnave, E., Marletto, V., Morse, A.P., Orfila, B., Rogel, P., Terres, J.-M., Thomson, M.C., 2004. Development of a European multimodal ensemble system for seasonal-to-interannual prediction. Bull. Am. Meteorol. Soc. 85 (6), 853–872. https://journals.ametsoc.org/view/journals/bams/85/6/bams-85-6-853.xml.

Papineau, J.M., 2001. Wintertime temperature anomalies in Alaska correlated with ENSO and PDO. Int. J. Climatol. 21, 1577–1592. https://doi.org/10.1002/joc.686.

Petrich, C., Eicken, H., Zhang, J., Krieger, J., Fukamachi, Y., Ohshima, K.I., 2012. Coastal landfast sea ice decay and breakup in northern Alaska: key processes and seasonal prediction. J. Geophys. Res. Oceans 117 (C2), C02003. https://doi.org/10.1029/2011JC007339.

Potter, R.E., Walden, J.T., 1981. Design and construction of sea ice roads in the Alaskan Beaufort Sea. In: 134th Annual Offshore Technology Conference, Houston, Texas, pp. 135–140.

Rigor, I.G., Wallace, J.M., Colony, R.L., 2002. Response of sea ice to the Arctic Oscillation. J. Clim. 15, 2648–2663. https://doi.org/10.1175/1520-0442(2002)015<2648:ROSITT>2.0.CO;2.

Saha, S., Moorthi, S., Wu, X., Wang, J., Nadiga, S., Tripp, P., Behringer, D., Hou, Y.T., Chuang, H.Y., Iredell, M., Ek, M., Meng, J., Yang, R., Mendez, M.P., Van Den Dool, H., Zhang, Q., Wang, W., Chen, M., Becker, E., 2014. The NCEP climate forecast system version 2. J. Clim. 27, 2185–2208. https://doi.org/10.1175/JCLI-D-12-00823.1.

Sampath, A., Bhatt, U.S., Bieniek, P.A., Ziel, R., York, A., Strader, H., Alden, S., Thoman, R., Brettschneider, B., Petrescu, E., Peng, P., Mitchell, S., 2021. Evaluation of seasonal forecasts for the fire season in interior Alaska. Weather Forecast. 36, 601–613. https://doi.org/10.1175/waf-d-19-0225.1.

Sigmond, M., Fyfe, J.C., Flato, G.M., Kharin, V.V., Merryfield, W.J., 2013. Seasonal forecast skill of Arctic Sea ice area in a dynamical forecast system. Geophys. Res. Lett. 40, 529–534. https://doi.org/10.1002/grl.50129.

Stroeve, J.C., Maslanik, J., Serreze, M.C., Rigor, I., Meier, W., Fowler, C., 2011. Sea ice response to an extreme negative phase of the Arctic Oscillation during winter 2009/2010. Geophys. Res. Lett. 38 https://doi.org/10.1029/2010GL045662.

Walsh, J.E., Brettschneider, B., Kettle, N.P., Thoman, R.L., 2021. An Analog Method for Seasonal forecasting in Northern High Latitudes. Atmos. Clim. Sci. 11, 469–485. https://doi.org/10.4236/ACS.2021.113028.

Yang, X.Y., Wang, G., Keenlyside, N., 2020. The Arctic Sea ice extent change connected to Pacific decadal variability. Cryosphere 14, 693–708. https://doi.org/10.5194/tc-14-693-2020.

Yu, Y., Stern, H., Fowler, C., Fetterer, F., Maslanik, J., 2014. Interannual variability of arctic landfast ice between 1976 and 2007. J. Clim. 27 (1), 227–243. https://doi.org/10.1175/JCLI-D-13-00178.1.

Zhang, J., Woodgate, R., Moritz, R., 2010. Sea ice response to atmospheric and oceanic forcing in the Bering Sea. J. Phys. Oceanogr. 40, 1729–1747. https://doi.org/10.1175/2010JPO4323.1.

Zhang, M., Perrie, W., Long, Z., 2019. Springtime North Pacific Oscillation and summer sea ice in the Beaufort Sea. Clim. Dyn. 53, 671–686. https://doi.org/10.1007/s00382-019-04627-1.

Zhao, J., Shu, Q., Li, C., Wu, X., Song, Z., Qiao, F., 2020. The role of bias correction on subseasonal prediction of Arctic Sea ice during summer 2018. Acta Oceanol. Sin. 39, 50–59. https://doi.org/10.1007/s13131-020-1578-0.